ACS APPLIED MATERIALS & INTERFACES

Research Article

www.acsami.org

Positive Role of Surface Defects on Carbon Nanotube Cathodes in Overpotential and Capacity Retention of Rechargeable Lithium–Oxygen Batteries

Shiting Huang,[†,‡] Wugang Fan,[†] Xiangxin Guo,*[,†] Fanhao Meng,[†] and Xuanyong Liu[†]

[†]State Key Laboratory of High Performance Ceramics and Superfine Microstructure, Shanghai Institute of Ceramics, Chinese Academy of Sciences, 1295 Dingxi Road, Shanghai 200050, China

[‡]Graduate School of the Chinese Academy of Sciences, Beijing 100039, China

Supporting Information

ABSTRACT: Surface defects on carbon nanotube cathodes have been artificially introduced by bombardment with argon plasma. Their roles in the electrochemical performance of rechargeable Li–O_2 batteries have been investigated. In batteries with tetraethylene glycol dimethyl ether (TEGDME)- and *N*-methyl-*N*-propylpiperidinium bis-(trifluoromethansulfonyl)imide (PP13TFSI)-based electrolytes, the defects increase the number of nucleation sites for the growth of Li_2O_2 particles and reduce the size of the formed particles. This leads to increased discharge capacity and reduced cycle overpotential. However, in the former batteries, the hydrophilic surfaces induced by the defects promote carbonate formation, which imposes a deteriorating effect on the cycle performance of the Li–O_2 batteries. In contrast, in the latter case, the defective cathodes promote Li_2O_2 formation without enhancing formation of carbonates on the cathode surfaces, resulting in extended cycle life. This is most probably attributable to the passivation effect on the functional groups of the cathode surfaces imposed by the ionic liquid. These results indicate that defects on carbon surfaces may have a positive effect on the cycle performance of Li–O_2 batteries if they are combined with a helpful electrolyte solvent such as PP13TFSI.

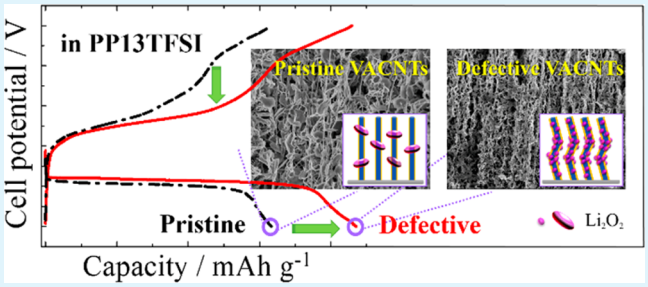

KEYWORDS: *surface defects, argon-plasma bombardment, carbonate species, lithium–oxygen batteries, carbon nanotubes, lithium peroxides*

INTRODUCTION

Rechargeable Li–air (or Li–O_2) batteries with nonaqueous electrolytes have been the focus in recent years because of their great potential for use as storage units with superhigh energy densities for electric vehicles and grid applications.[1−9] A typical Li–O_2 battery consists of a Li anode, an oxygen diffusion cathode, a nonaqueous lithium ion conducting electrolyte, and a (flow or static) oxygen atmosphere. During discharge, the large capacity results from deposition of a large amount of Li_2O_2 crystals on the cathode surface via the half-reaction $2Li^+ + 2e^- + O_2 \rightarrow Li_2O_2$.[10−12] Since these products are insulating and not soluble in the electrolyte, it is highly demanded that the cathodes are conductive with sufficient space to accommodate the solid products.[13−16] During charge, the formed Li_2O_2 crystals need to be decomposed via the half-reaction $Li_2O_2 \rightarrow 2Li^+ + 2e^- + O_2$,[10−12] which also calls for cathodes with high electron conductivity. As a result, carbon-based cathodes have been widely used for nonaqueous Li–O_2 batteries because of their high conductivity, large surface area, great porosity, light weight, and low cost.[17−22]

Unfortunately, as many previous papers have pointed out, carbon-based cathodes might not be stable during cell operation. For instance, Thotiyl et al.[23] reported that the carbon can be oxidatively decomposed to form Li_2CO_3 upon charging above 3.5 V, especially for hydrophilic carbons, which become less stable against Li_2O_2 and more catalytically active toward decomposition of the ether-based electrolytes compared with hydrophobic carbons. McCloskey and co-workers reported that a monolayer of Li_2CO_3 could be formed at the C–Li_2O_2 and Li_2O_2–electrolyte interfaces,[24,25] which is consistent with the results on carbonate evolution during discharge and charge as reported by Black et al.[26] In addition, Itkis et al.[27] found that superoxide radicals react with functional groups and defects on the carbon surface to form epoxy groups and carbonates, limiting the cell rechargeability.

In contrast, Nakanishi and co-workers[28,29] reported that defects on carbon surfaces are beneficial for improvement of battery performance. Careful examination of the above research reports showed that Nakanishi et al.'s results were obtained using batteries with ionic-liquid-based electrolytes, while other

Received: September 24, 2014
Accepted: November 14, 2014
Published: November 14, 2014

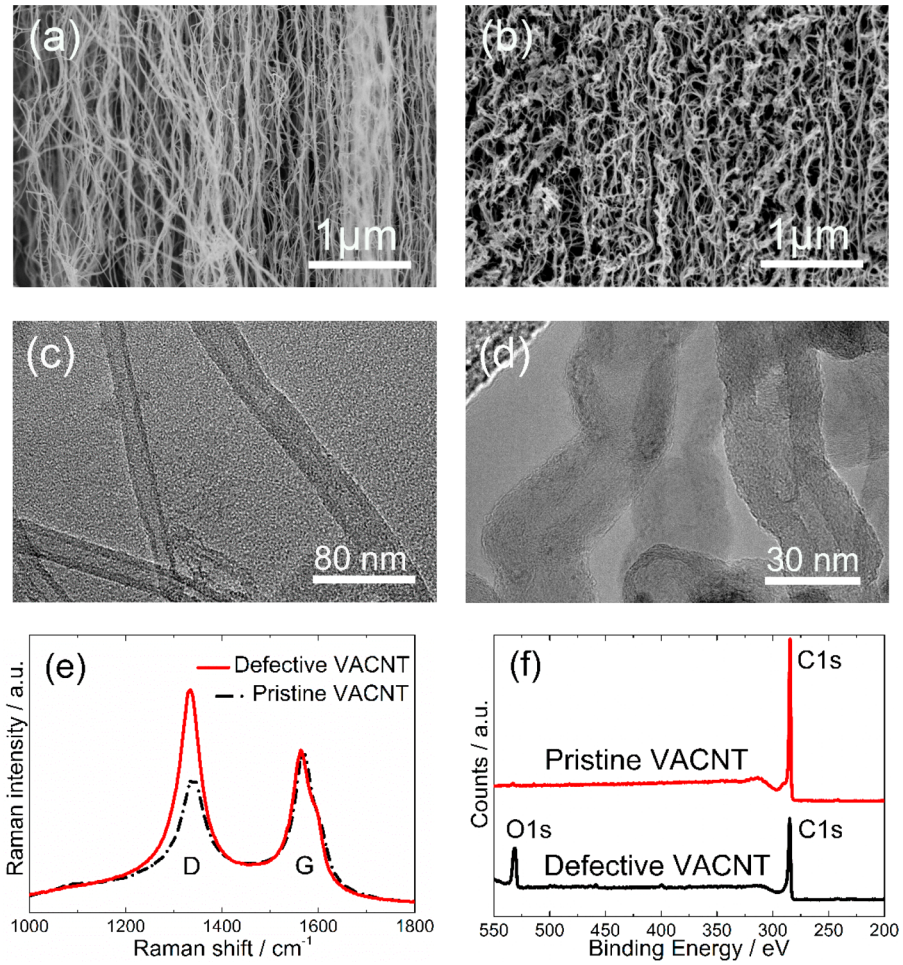

Figure 1. (a, b) Typical SEM images of (a) pristine and (b) defective VACNTs. (c, d) TEM images of (c) pristine and (d) defective VACNTs. (e) Raman spectra and (f) XPS spectra of the defective VACNTs in comparison with those of pristine VACNTs.

reports used ether-based ones. This indicates that the role of defects on the carbon surface in battery performance should be examined in combination with the electrolyte.

Therefore, in this work, defects were artificially created on the surfaces of carbon nanotube (CNT)-based cathodes by bombardment with argon plasma. The effect of the interplay between the defects and the electrolytes [including tetraethylene glycol dimethyl ether (TEGDME)- and *N*-methyl-*N*-propylpiperidinium bis(trifluoromethansulfonyl)imide (PP13TFSI)-based electrolytes] on the overpotential and capacity retention of Li−O_2 cells was investigated. It was found that in comparison with pristine CNT cathodes, surface defects increase the number of nucleation sites and reduce the size of Li_2O_2 particles in both TEGDME- and PP13TFSI-based cells, leading to increased discharge capacities and decreased overpotentials in the first discharge−charge cycle. In the TEGDME-based cells, however, the defects enhance the side reactions and promote the formation of Li_2CO_3, which worsens the cell cyclability. In contrast, in the PP13TFSI-based ones, the defects do not increase the Li_2CO_3 formation. This effect improves the cycle stability during cell operation. The underlying mechanism is most probably attributable to the protection effect on the carbon surfaces led by the molecules of the ionic liquid.

EXPERIMENTAL SECTION

Each Li−O_2 cell of the Swagelok type was assembled in an Ar-filled glovebox with oxygen and moisture levels below 0.1 ppm; the cells consisted of a 0.5 mm thick lithium foil anode, a vertically aligned CNT (VACNT) cathode, and a Whatman glass fiber separator soaked with the electrolyte. The pristine VACNTs, which were grown on stainless steel (SS) by chemical vapor deposition, were purchased from Microphase Co. Ltd. (Tsukuba, Japan).[30] The loading amount of VACNTs grown on SS was approximately 2 mg cm^{-2}. Defects on the surfaces of the VACNTs were artificially made by the implantation of argon plasma into the pristine VACNTs using plasma immersion ion implantation (PIII) technology.[31] The main arc current and pulsed high voltage applied were synchronized at a pulsing frequency of 30 kHz. The VACNTs were treated for 30 min with a radiofrequency argon plasma source at a bias of −300 V, and the sample stage was actively cooled by circulating water to keep the sample temperature at 25 °C. Both the pristine and treated VACNTs were dried at 80 °C under vacuum for 48 h before the cell assembly. $LiClO_4$ (99.99% trace metal basis, Aldrich) and the ionic liquid PP13TFSI (Kanto Chemical Corporation) in battery grade were baked at 80 °C under vacuum for 24 h. TEGDME (Aldrich) and PP13TFSI with water contents below 5 ppm, as measured using a Metrohm 831 KF coulometer, were used as the electrolyte solvents.

After the assembly, the cells were sealed in gastight containers with inlet and outlet tubes for oxygen exchange. Under a flowing O_2 atmosphere the cells were rested for 4 h first, and then the discharge and charge measurements were conducted using an Arbin BT 2000 cycler.

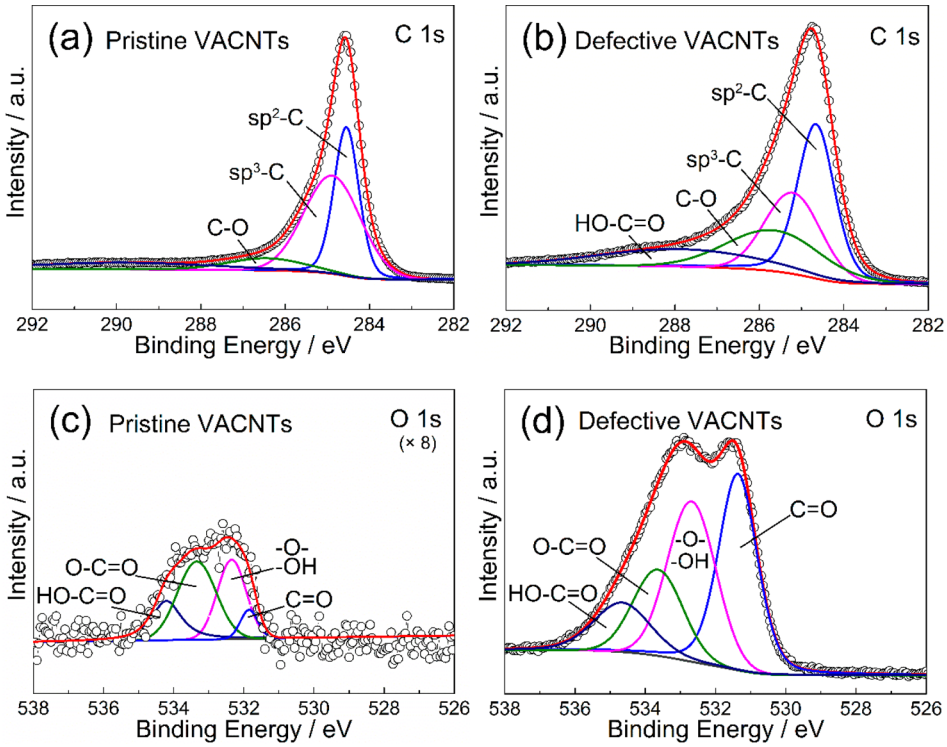

Figure 2. XPS patterns of the (a, b) C 1s and (c, d) O 1s binding energy regions of (a, c) pristine and (b, d) defective VACNTs. The O 1s intensity of pristine VACNTs is magnified 8 times.

After the measurements, the discharged and charged VACNT cathodes were removed from the batteries in the Ar-filled glovebox and rinsed with anhydrous CH_3CN (i.e., <4 ppm H_2O). This can dissolve the residual electrolytes on the cathodes and then effectively purge them away, and it is chemically stable toward the reaction products including Li_2O_2 and Li_2CO_3, thus benefiting the study of the reactions occurring at the cathodes. In addition, the excess CH_3CN is volatile to move away from the cathodes. Then cathodes were dried on a filter paper under vacuum and characterized by X-ray diffraction (XRD) (Bruker D8 Discover), field-emission scanning electron microscopy (SEM) (FEI Magellan 400), and X-ray photoelectron spectroscopy (XPS). More details on characterizations of the cathodes and composition analysis can be found in our previous work.[32]

Raman spectra were recorded on a Thermo DXR spectrometer with an excitation wavelength of 532 nm. Cyclic voltammetry (CV) measurements were performed with an electrochemical workstation (Autolab) utilizing homemade three-electrode electrochemical cells.[33] Each cell employed a dual reference electrode, a platinum mesh counter electrode, and a glassy carbon working electrode in a diameter of 3 mm. The dual reference electrode consisted of parallel Ag/Ag^+ and platinum wire electrodes. It can reduce the impedance as well as the response time to the potentiostat, thus improving the signal-to-noise ratio during the measurements.[34] The Ag/Ag^+ electrode consisted of a silver wire immersed in an electrolyte of 0.1 M $AgCF_3SO_3$/TEGDME in a glass tube and separated with a Vycor frit. The potential of the reference electrode was measured against a Li foil in an Ar-filled glovebox and was found to be −3.6 V vs Li/Li^+ with respect to 0.1 M $LiClO_4$ in TEGDME. The working electrodes were made by coating pristine or defective VACNTs on the surface of glassy carbon and then fixed with Nafion solution and finally dried at 80 °C for 12 h under vacuum.

RESULTS AND DISCUSSION

Characterization of Defects on Surfaces of the VACNT Cathode. Figure 1a,b shows the morphologies of typical pristine and defective VACNT cathodes, respectively, as detected by SEM. It can be seen that while most of the pristine CNTs are straight and separately distributed, the defective CNTs are bent and tending to connect. Transmission electron microscopy (TEM) observations revealed that the surfaces of the pristine CNTs are smooth, whereas those of the defective ones have many kinks (Figure 1c,d). High-resolution TEM indicated that formation of the kinks is due to dislocations between the multiple carbon layers led by the bombardment with Ar plasma (Figure S1 in the Supporting Information). Consistently, Raman spectroscopy measurements (Figure 1e) showed that the ratio of the peak intensities of the D and G bands greatly increases after bombardment of the VACNTs, clearly indicating that the amount of defect sites significantly increases.[35,36] XPS was used to study the chemical identities of functional groups on the pristine and defective VACNTs. As shown in Figure 1f, the O/C ratio is much larger for the defective VACNTs than for the pristine ones. It is proposed that after the Ar bombardment, the C−C covalent bonds on the CNT surfaces were broken off, forming many dangling carbon bonds. These dangling bonds might absorb oxygen functional groups that exist either in the residual atmosphere of the vacuum chamber during bombardment or in the protection atmosphere during transfer.

In addition, high-resolution XPS scans revealed that the peak intensities of oxygen species, including carboxylic (534.4 ± 0.1 eV), ester (533.4 ± 0.1 eV), hydroxyl/epoxide (532.5 ± 0.2 eV), and carbonyl groups (531.6 ± 0.1 eV), obviously increased after the Ar bombardment in comparison with the O 1s spectra of the pristine VACNTs (Figure 2c,d). This corresponds to the higher hydroxyl/epoxide (286.1 ± 0.2 eV) and carboxylic (288.9 ± 0.2 eV) peak intensities in the C 1s spectrum of the defective VACNTs (Figure 2b) compared with that of the pristine VACNTs (Figure 2a).

Because of these oxygen functional groups introduced by the Ar bombardment, the water contact angle with the VACNT

cathode surface changes from 140.47° to 43.90° (Figure 3), which represents a clear transition from the hydrophobic to the hydrophilic property.

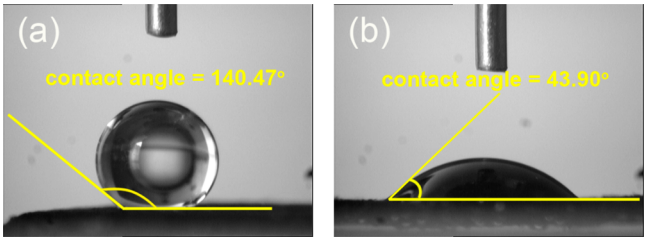

Figure 3. Water contact angles with the surfaces of (a) pristine and (b) defective VACNT cathodes.

Interplay between the Surface Defects and the TEGDME-Based Electrolyte. The first discharge and charge behaviors of the cells with pristine and defective VACNT cathodes in TEGDME-based electrolytes were investigated comparatively. The typical curves measured over the potential range of 2−4.5 V at a current density of 0.1 mA cm^{-2} are shown in Figure 4a. From the figure it is obvious that the discharge capacity of ∼5800 mA h g^{-1} with the defective VACNTs is much larger than that of ∼1900 mA h g^{-1} with the pristine ones. The CV measurements also indicate that the defective VACNTs show a higher cathodic current than the pristine ones (Figure 4b). The two oxygen reduction reaction (ORR) peaks in the CV curves can be attributed to the processes of LiO_2 and Li_2O_2 formation.[37] These results indicate that defects on the VACNTs promote the ORR reaction, leading to an increased discharge capacity. In addition, an obvious reduction in the discharge overpotential in the case of the defective VACNTs can be seen in both Figure 4a and Figure 4b. The peak intensity corresponding to the decomposition of Li_2CO_3[37] also increases in the case of defective VACNTs, as shown in Figure 4b. The explanations for these phenomena will be given in the following.

In order to clarify the role of defects on the VACNT surfaces in the formation and decomposition of the reaction products, the chemical and morphological changes of cathodes after they were discharged to 2.0 V and recharged to 4.5 V were investigated by SEM, XRD, and XPS. As shown in Figure 5a,b, after the discharge to 2.0 V, while many abacus-ball-shaped particles with sizes of ∼200 nm grown around the nanotubes can be found for the pristine VACNT cathode, a large number of particles smaller than 50 nm are grown around the defective VACNTs. XRD measurements confirmed that the discharge products are dominated by crystalline Li_2O_2, as shown in Figure S2a,b. It is clear that the introduced defects lead to the decreased size and increased numerical density of the Li_2O_2 particles, in agreement with the increased discharge capacity. Moreover, as shown in Figure 5e,f, the XPS results indicated that although a small amount of Li_2CO_3 was formed on the pristine VACNTs after the full discharge, its amount increased substantially in the case of the defective VACNTs. These results are consistent with the increased peak intensity of Li_2CO_3 decomposition shown in Figure 4b, clearly indicating that the defects enhance the side reactions during discharge. It has been proven that hydrophobic carbon is relatively stable upon discharge, having a minor direct chemical reaction with the TEGDME-based electrolyte and forming only a small amount of carbonate species.[23] This is consistent with our results. Hydrophilic carbon is less stable and more catalytically active toward electrolyte decomposition.[23] Therefore, we can draw the conclusion that the defects on VACNTs promote decomposition of the electrolyte during discharge, increasing the amount of Li_2CO_3 deposited on the cathode surfaces. However, the hydrophobic carbon nanotubes with fewer defects in our work possess fewer nucleation sites, leading to a smaller capacity and larger discharge products in the lithium−oxygen battery.

After recharge to 4.5 V, the residual materials on the surfaces of the pristine VACNTs become much less (Figure 5c). Meanwhile, XRD measurements indicate that the peak corresponding to the crystalline Li_2O_2 disappears (Figure S2a). The XPS results also indicate the existence of negligible carbonates (Figure 5e). These results mean that after the recharge to 4.5 V both Li_2O_2 and carbonates resulting from the electrolyte decomposition can be greatly removed from the pristine VACNTs. In contrast, after the recharge to 4.5 V a lot of materials are still coated on the defective VACNTs (Figure 5d). XRD measurements reveal no existence of the crystalline Li_2O_2 (Figure S2b). Instead, the XPS results show signals of carbonate species, as can be seen in Figure 5f. It should be that the peak at 287 eV in Figure 5f is a hint of residual electrolyte on the cathode, which was also observed in the previous work.[30] These results indicate that the introduced defects promote the formation of carbonates during charge. This could be attributed to the high reactivity of Li_2O_2 particles with the reduced size led by the defects.

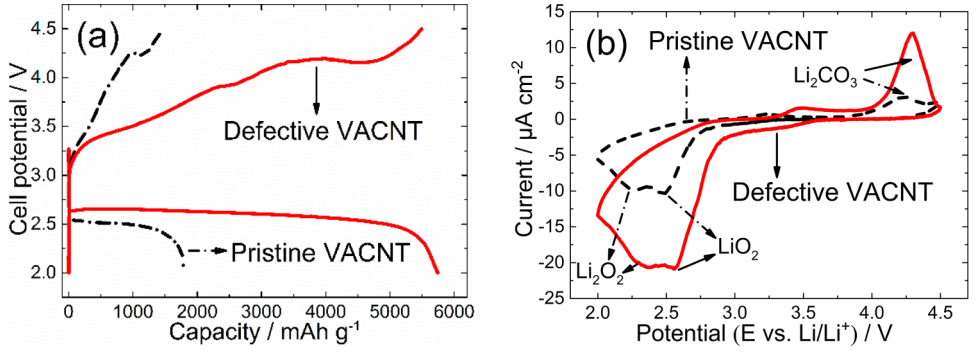

Figure 4. (a) First full cycle curves for the TEGDME-based cells with pristine and defective VACNT cathodes measured at a current density of 0.1 mA cm^{-2} over the voltage range of 2.0−4.5 V. (b) CV curves for the pristine and defective VACNT cathodes tested in an Ar/O_2 (80:20 v/v) atmosphere between 2.0 and 4.5 V vs Li/Li^+ at a scan rate of 20 mV s^{-1}.

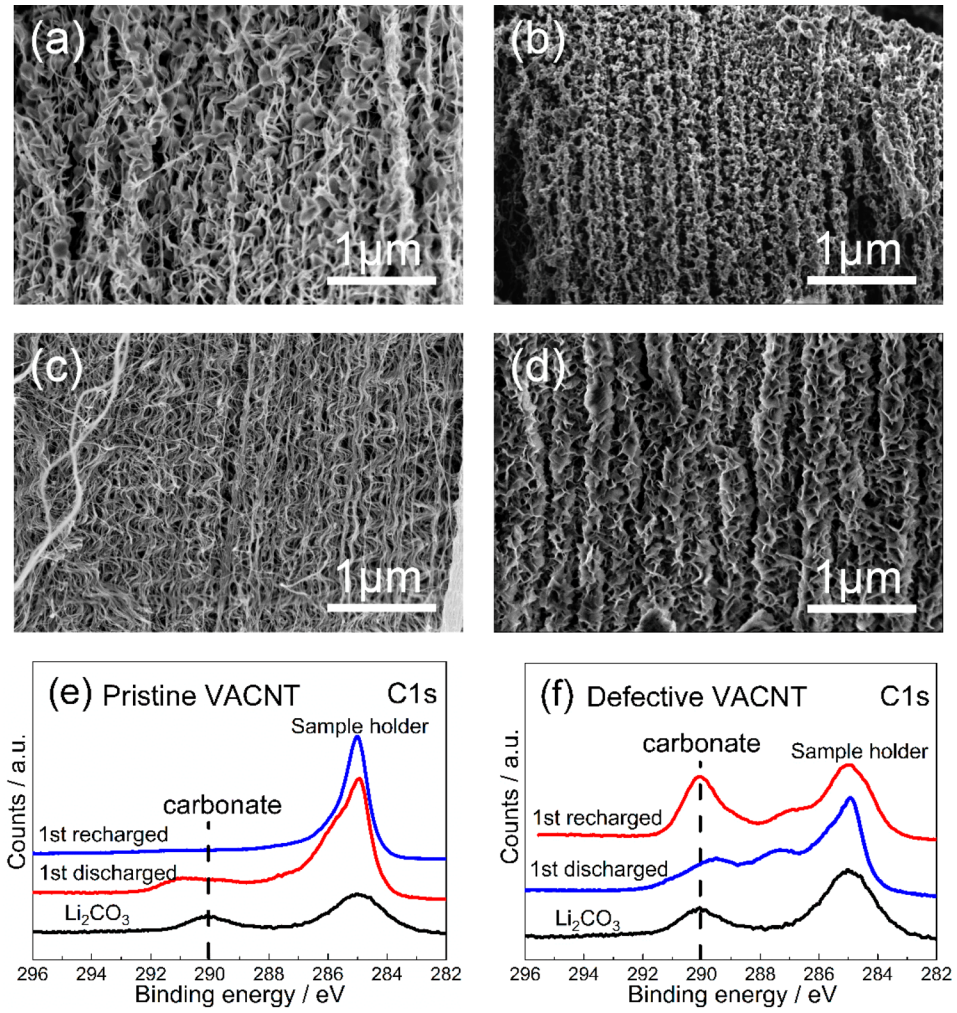

Figure 5. (a–d) SEM images of the pristine and defective VACNT cathodes disassembled from the TEGDME-based batteries after the first discharge and recharge processes: (a) pristine and (b) defective VACNTs discharged to 2.0 V; (c) pristine and (d) defective VACNTs recharged to 4.5 V. (e, f) XPS spectra of (e) pristine and (f) defective VACNTs after the first discharge to 2.0 V and recharge to 4.5 V.

Consequently, when being operated with a discharge capacity cutoff of 1000 mA h g^{-1} and a charge cutoff potential of 4.5 V at a current density of 0.1 mA cm^{-2}, the cells with the defective VACNT cathodes exhibit a slightly lower discharge overpotential than those with the pristine ones, as can be seen in Figure 6a. Meanwhile, the charge overpotential of the defective VACNTs increases, becoming larger than that of the pristine ones after 10 cycles. Therefore, the cells with the defective VACNTs run fewer cycles than those with the pristine ones as the discharge capacity is maintained as 1000 mA h g^{-1} (Figure 6b). This is attributed to the fact that the defective VACNTs promote electrolyte decomposition and oxidation of carbon during discharge and charge, forming a great deal of residual carbonates on the cathode surfaces. These carbonate species cause passivation of the active cathodes, thus dramatically deteriorating the cell cyclability.

It should be noted that under the condition of complete discharge (i.e., Figure 4a), the overpotentials of defective VACNTs are much lower than those of pristine ones. Under the condition of a discharge cutoff capacity of 1000 mA h g^{-1} (i.e., Figure 6a), the overpotentials for the defective and pristine VACNTs are similar. In the former case, the complete discharge leads to the large capacity as well as the large number of Li_2O_2 particles. While the typical particle size for the pristine VACNTs is approximately 200 nm, that for the defective VACNTs is only ~50 nm. The smaller particles are obviously easier to decompose, thus resulting in the lower overpotential. In the latter case, the sizes of Li_2O_2 particles for both pristine and defective VACNTs are expected to be similar because of the limited discharge capacity. This leads to the similar overpotentials observed in Figure 6a.

Interplay between the Surface Defects and the PP13TFSI-Based Electrolyte. The first discharge and charge curves of the cells with the pristine and defective VACNTs cathodes in the PP13TFSI-based electrolytes, measured between 2.0 and 4.5 V at a current density of 0.1 mA cm^{-2}, are shown in Figure 7a. From the figure it can be seen that the discharge capacity of the defective VACNTs is larger than that of the pristine ones and that the overpotential for the former is smaller than that for the latter. Figure 7b shows the cycle performance of the cells operated with a limited discharge capacity of 1000 mA h g^{-1}. It can also be found that the cycle overpotential of cells with the defective VACNTs cathodes is slightly smaller than that for the pristine VACNTs cathodes. This is consistent with the fact that the defects on VACNTs lead to easy formation and decomposition of Li_2O_2.

To clarify the role of defects on the VACNT surfaces in the interplay between the cathode and the PP13TFSI-based

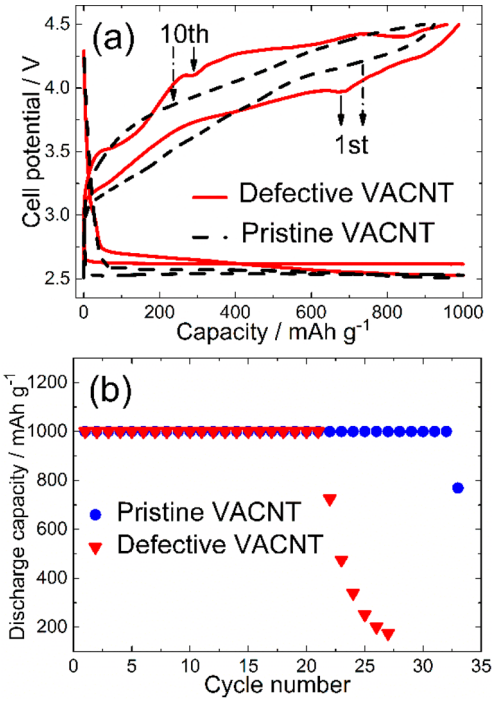

Figure 6. (a) First and 10th cycle curves of TEGDME-based batteries with pristine and defective VACNT cathodes tested at a current density of 0.1 mA cm^{-2} with a capacity cutoff of 1000 mA h g^{-1}. (b) Discharge capacity as a function of cycle number for the pristine and defective VACNT cathodes in the TEGDME-based electrolyte.

electrolyte, SEM, XRD, and XPS were used to investigate the chemical and morphological changes of the cathodes after they were discharged to 2.0 V and recharged to 4.5 V. As shown in Figure 8a,b, after discharging, many abacus-ball-shaped particles were grown around the nanotubes of the pristine VACNT cathode. In contrast, a greater number of particles with smaller sizes were grown around the defective VACNTs. XRD measurements (Figure S3a,b) confirmed that the discharge products are mainly crystalline Li_2O_2. These results are in agreement with the conclusion that the introduced defects decrease the size of Li_2O_2 particles and increase the number density of the particles, leading to the increased discharge capacity and decreased overpotential. Comparison of the discharge products in the two kinds of electrolytes (Figure 5b with Figure 8b) shows that the Li_2O_2 particles in the TEGDME-based electrolyte are smaller in size and have a higher density than those in the PP13TFSI-based electrolyte. This result indicates that the TEGDME-based electrolyte favors the formation of smaller-sized Li_2O_2 particles in larger numbers compared with the PP13TFSI-based electrolyte, in accord with the observed discharge capacities. However, the XPS results (Figure 8e) show a negligible amount of Li_2CO_3 formed in PP13TFSI, which is different from the situation in the case of TEGDME (Figure 5e). This is consistent with the fact that the PP13TFSI-based electrolytes have better stability than the TEGDME-based ones during discharge.[30]

On the basis of XRD (Figures S2 and S3), the crystallinity of Li_2O_2 seems similar for both pristine and defective VACNTs in different solvents. From SEM, we can observe that the size of Li_2O_2 particles formed in the TEGDME-based electrolyte (Figure 5a,b) after full discharge to 2 V are smaller than in the PP13TFSI-based electrolyte (Figure 8a,b). Meanwhile, the size of the Li_2O_2 particles formed on pristine VACNTs (Figures 5a and 8a) is larger than that on defective VACNTs (Figure 5b and 8b) in both electrolytes. It should be noted that these results provide information only about the particle size rather than crystalline size. For clarification of the crystalline size, more investigations are needed.

Figure 8c,d shows SEM images of the surface morphologies of the pristine and defective VACNTs after recharge to 4.5 V, respectively. It can be seen that in both cases the residual products are negligible. Correspondingly, XRD measurements reveal that the peaks arising from crystalline Li_2O_2 disappear (Figure S3a,b). This is in accord with the conclusion that the recharge to 4.5 V can decompose most of the discharge products for both cases. More interestingly, Figure 8f shows that the Li_2CO_3 signals for both pristine and defective VACNTs after recharge in the PP13TFSI-based cells are negligible. Since in the TEGDME-based cells the peak intensity of Li_2CO_3 obviously increases after the recharge (Figure 5f), the above results indicate that in comparison with TEGDME the PP13TFSI-based electrolyte most probably has a protecting effect on the surfaces of defective VACNTs. This is not unreasonable considering that the cations in the ionic liquid can interact with the defects and form a monolayer on the surface of the VACNTs.[38] The ionic liquid can depress the formation of side products such as Li_2CO_3 through the passivation layer for both pristine and defective VACNTs. Moreover, the defects on VACNTs may act as additional nucleation sites for Li_2O_2, which leads to the reduced particle size. These factors will promote the cycle life of the defective VACNTs in the ionic liquid. In addition, the surface hydrophobicity or hydrophilicity

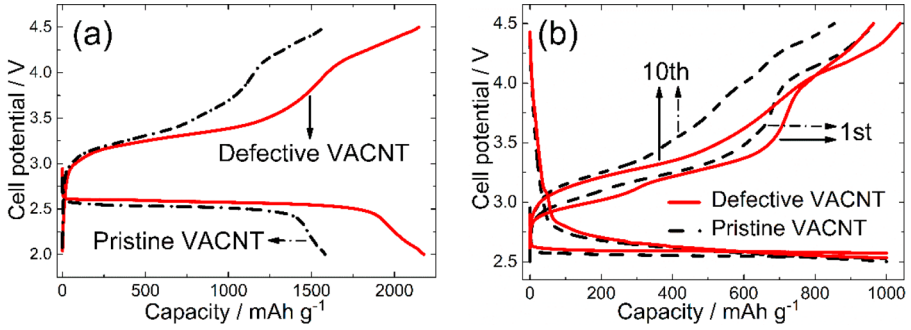

Figure 7. (a) First full cycle curves for PP13TFSI-based cells with pristine and defective VACNT cathodes measured at a current density of 0.1 mA cm^{-2} over the voltage range of 2.0–4.5 V. (b) First and 10th cycle curves of PP13TFSI-based batteries with pristine and defective VACNT cathodes tested at a current density of 0.1 mA cm^{-2} with a capacity cutoff of 1000 mA h g^{-1}. All of the PP13TFSI-based cells were measured at 60 °C.

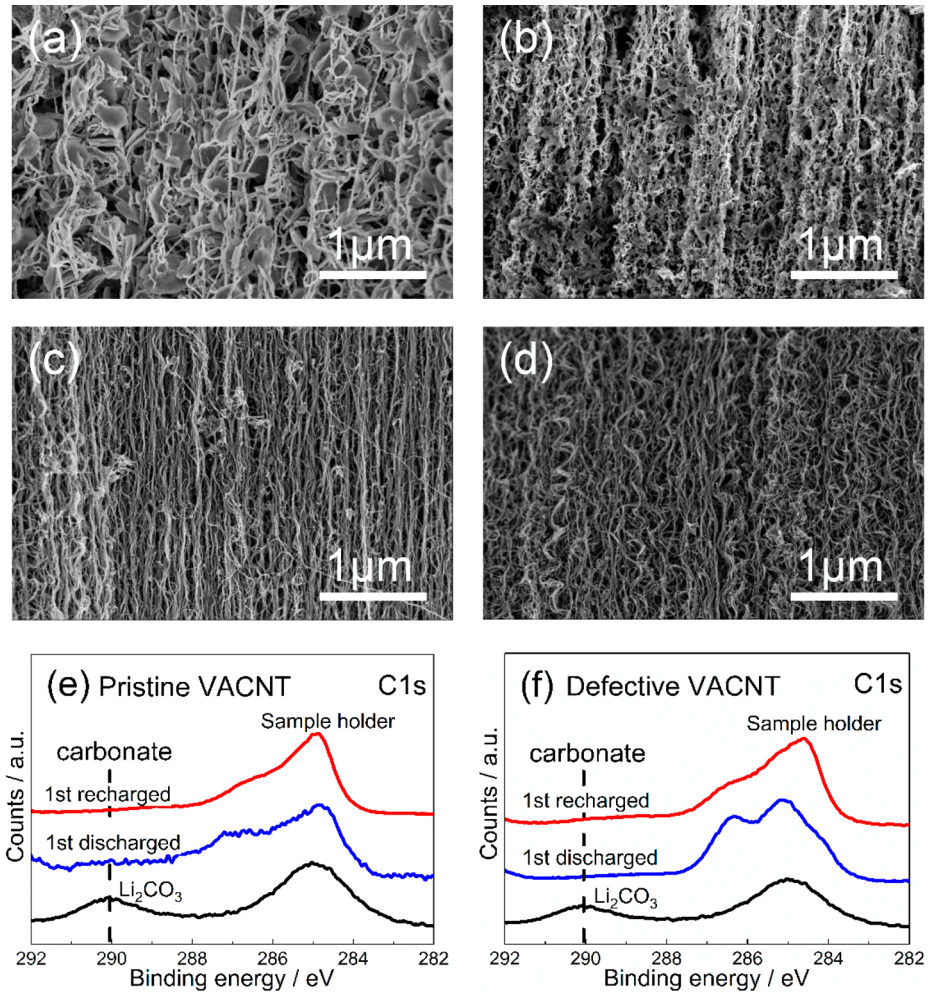

Figure 8. (a–d) SEM images of pristine and defective VACNT cathodes disassembled from PP13TFSI-based batteries after the first discharge and recharge processes: (a) pristine and (b) defective VACNTs discharged to 2.0 V; (c) pristine and (d) defective VACNTs recharged to 4.5 V. (e, f) XPS spectra of (e) pristine and (f) defective VACNT surfaces after the first discharge to 2.0 V and recharge to 4.5 V.

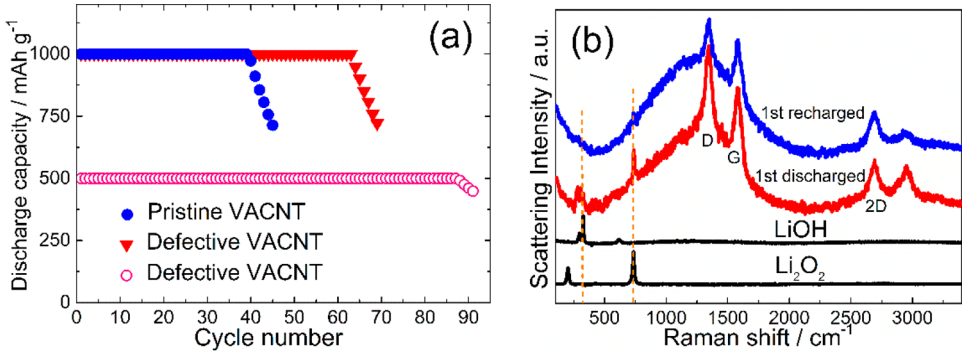

Figure 9. (a) Discharge capacity as a function of cycle number for the pristine and defective VACNT cathodes in the PP13TFSI-based electrolyte. (b) Raman spectra of defective VACNT cathodes after the first discharge and recharge processes.

may have a great influence on the side reaction between the cathode and the electrolyte. According to our results, hydrophobic carbon is more stable and less active with the TEGDME-based electrolyte than hydrophilic carbon, thus forming less side products in the former case. This is in agreement with the results presented in ref 23. Nevertheless, in the PP13TFSI-based electrolyte, the difference in the influence of hydrophobic and hydrophilic VACNTs on side reactions is negligible because of the good stability of the electrolyte solvent. These results indicate that the influence of the surface property on the reaction should be considered under the specific electrolyte system. Overall, the introduced defects on the VACNTs surfaces lead to the easy formation and decomposition of Li_2O_2 by decreasing the particle size of Li_2O_2. Moreover, PP13TFSI improves the stability of the electrolyte as well as the oxygen cathode. All of these factors consequently reduce the cycle overpotential and improve the cycle stability.

Consistently, as shown in Figure 9a, the cells with pristine and defective VACNT cathodes in the PP13TFSI-based electrolyte run 39 and up to 63 cycles, respectively, as the discharge capacity is maintained at 1000 mA h g^{-1}. It should be noted that the pristine VACNTs in TEGDME electrolyte terminate after 32 cycles under the same capacity cutoff. This result is consistent with the better stability of the PP13TFSI-based electrolytes compared with the TEGDME-based ones. Furthermore, further reducing the depth of discharge to 500 mA h g^{-1} allows the cycle number to be extended to approximately 90, as shown in Figure 9a. Comparing the discharge−charge curves for the defective VACNTs in different electrolytes, we can observe that the discharge capacity in the PP13TFSI-based electrolyte (Figure 7a) is lower than that in the TEGDME-based one (Figure 4a). It is known that the discharge capacity is dependent on the amount of formed products. On one hand, the oxygen solubility is expected to be higher in TEGDME than in PP13TFSI, which can promote the formation of L_2O_2. On the other hand, TEGDME is more reactive with defective VACNTs than PP13TFSI. This causes more lithium carbonates to form in the case of TEGDME. Both factors may lead to the larger discharge capacity in TEGDME than in PP13TFSI. In the previous report,[39] it was pointed out that the LiOH might be formed as a result of extraction of H from PP13TFSI. To examine whether this is also the case here, Raman spectra were measured on the first discharged and recharged products for the cells with the defective VACNTs cathodes. As shown in Figure 9b, Li_2O_2 and LiOH formed after discharge and decomposed after recharge can be clearly seen. This is consistent with the results in ref 39, indicating that the stability of PP13TFSI still needs to be improved for construction of further long-lived Li−O_2 cells.

CONCLUSIONS

Artificial defects have been introduced on surfaces of the carbon nanotube cathodes, which leads to an increased amount of defect sites and the transition from the hydrophobic to hydrophilic property. The interplays between the defective cathodes and the TEGDME- and PP13TFSI-based electrolytes have been investigated. It was found that in both types of electrolytes the defects act as additional nucleation sites for Li_2O_2 formation, leading to an increase in the density of Li_2O_2 particles along with a size decrease of the individual particles. Correspondingly, the cells with the defective VACNT cathodes show increased discharge capacities and reduced cycle overpotential in the case of full discharge and charge operation. However, the defects on VACNTs enhance the formation of side products (i.e., carbonate species) by oxidation of hydrophilic carbon and decomposition of the TEGDME electrolyte, reducing the cycle life of the Li−O_2 cells. In contrast, such an effect does not exist in the cells with the PP13TSFI-based electrolyte, which is most probably attributable to a passivation effect on the functional groups of the cathode surfaces imposed by the ionic liquid. The results here clearly indicate that the interplay between the cathode surface and the electrolyte should be considered for improving the performance of Li−O_2 batteries. Defects on the cathode surfaces could be helpful for the battery performance if the interface between the cathode and the electrolyte is suitably manipulated.

ASSOCIATED CONTENT

Supporting Information

TEM images of pristine and defective VACNTs (Figure S1) and XRD scans of pristine and defective VACNT cathodes disassembled from the TEGDME-based (Figure S2) and PP13TFSI-based (Figure S3) batteries after the first discharge to 2.0 V and the first recharge to 4.5 V. This material is available free of charge via the Internet at http://pubs.acs.org.

AUTHOR INFORMATION

Corresponding Author

*Tel.: 0086-21-52411032. Fax: 0086-21-52411802. E-mail: XXGuo@mail.sic.ac.cn.

Notes

The authors declare no competing financial interest.

ACKNOWLEDGMENTS

This work was supported by the National Key Basic Research Program of China (2014CB921004), the Key Project of the Chinese Academy of Sciences (KGZD-EW-202-2), the Science Foundation for Young Researchers of the State Key Laboratory of High Performance Ceramics and Superfine Microstructures (SKL201104), and the Natural Science Foundation of Shanghai (14ZR1445600).

REFERENCES

(1) Bruce, P. G.; Freunberger, S. A.; Hardwick, L. J.; Tarascon, J. M. Li−O_2 and Li−S Batteries with High Energy Storage. *Nat. Mater.* **2012**, *11*, 19−29.

(2) Lu, Y. C.; Gallant, B. M.; Kwabi, D. G.; Harding, J. R.; Mitchell, R. R.; Whittingham, M. S.; Shao-Horn, Y. Lithium−Oxygen Batteries: Bridging Mechanistic Understanding and Battery Performance. *Energy Environ. Sci.* **2013**, *6*, 750−768.

(3) Black, R.; Adams, B.; Nazar, L. F. Non-Aqueous and Hybrid Li−O_2 Batteries. *Adv. Energy Mater.* **2012**, *2*, 801−815.

(4) Li, F.; Ohnishi, R.; Yamada, Y.; Kubota, J.; Domen, K.; Yamada, A.; Zhou, H. Carbon Supported TiN Nanoparticles: An Efficient Bifunctional Catalyst for Non-Aqueous Li−O_2 Batteries. *Chem. Commun.* **2013**, *49*, 1175−1177.

(5) Xia, C.; Waletzko, M.; Peppler, K.; Janek, J. Silica Nanoparticles as Structural Promoters for Oxygen Cathodes of Lithium−Oxygen Batteries. *J. Phys. Chem. C* **2013**, *117*, 19897−19904.

(6) Nasybulin, E. N.; Xu, W.; Mehdi, B. L.; Thomsen, E.; Engelhard, M. H.; Masse, R. C.; Bhattacharya, P.; Gu, M.; Bennett, W.; Nie, Z.; Wang, C.; Browning, N. D.; Zhang, J. G. Formation of Interfacial Layer and Long-Term Cyclability of Li−O_2 Batteries. *ACS Appl. Mater. Interfaces* **2014**, *6*, 14141−14151.

(7) Lu, Y. C.; Gasteiger, H. A.; Shao-Horn, Y. Catalytic Activity Trends of Oxygen Reduction Reaction for Nonaqueous Li−Air Batteries. *J. Am. Chem. Soc.* **2011**, *133*, 19048−19051.

(8) Guo, X. X.; Huang, S. T.; Zhao, N.; Cui, Z. H.; Fan, W. G.; Li, C. L.; Li, H. Rapid Development and Critical Issues of Secondary Lithium−Air Batteries. *J. Inorg. Mater.* **2014**, *29*, 113−123.

(9) Girishkumar, G.; McCloskey, B. D.; Luntz, A. C.; Swanson, S.; Wilcke, W. Lithium−Air Battery: Promise and Challenges. *J. Phys. Chem. Lett.* **2010**, *1*, 2193−2203.

(10) Bhatt, M. D.; Geaney, H.; Nolan, M.; O'Dwyer, C. Key Scientific Challenges in Current Rechargeable Non-Aqueous Li−O_2 Batteries: Experiment and Theory. *Phys. Chem. Chem. Phys.* **2014**, *16*, 12093−12130.

(11) Hassoun, J.; Jung, H. G.; Lee, D. J.; Park, J. B.; Amine, K.; Sun, Y. K.; Scrosati, B. A Metal-Free, Lithium-Ion Oxygen Battery: A Step Forward to Safety in Lithium−Air Batteries. *Nano Lett.* **2012**, *12*, 5775−5779.

(12) Zhang, K. J.; Zhang, L. X.; Chen, X.; He, X.; Wang, X. G.; Dong, S. M.; Gu, L.; Liu, Z. H.; Huang, C. S.; Cui, G. L. Molybdenum

Nitride/N-Doped Carbon Nanospheres for Lithium−O_2 Battery Cathode Electrocatalyst. *ACS Appl. Mater. Interfaces* **2013**, *5*, 3677−3682.
(13) Xia, C.; Waletzko, M.; Chen, L.; Peppler, K.; Klar, P. J.; Janek, J. Evolution of Li_2O_2 Growth and Its Effect on Kinetics of Li−O_2 Batteries. *ACS Appl. Mater. Interfaces* **2014**, *6*, 12083−12092.
(14) Chen, Y.; Li, F.; Tang, D.-M.; Jian, Z.; Liu, C.; Golberg, D.; Yamada, A.; Zhou, H. Multi-Walled Carbon Nanotube Papers as Binder-Free Cathodes for Large Capacity and Reversible Non-Aqueous Li−O_2 Batteries. *J. Mater. Chem. A* **2013**, *1*, 13076−13081.
(15) Ellis, B. L.; Lee, K. T.; Nazar, L. F. Positive Electrode Materials for Li-Ion and Li-Batteries. *Chem. Mater.* **2010**, *22*, 691−714.
(16) Zhou, K.; Zhou, W.; Liu, X.; Wang, Y.; Wan, J.; Chen, S. Nitrogen Self-Doped Porous Carbon from Surplus Sludge as Metal-Free Electrocatalysts for Oxygen Reduction Reactions. *ACS Appl. Mater. Interfaces* **2014**, *6*, 14911−14918.
(17) Byon, H. R.; Gallant, B. M.; Lee, S. W.; Shao-Horn, Y. Role of Oxygen Functional Groups in Carbon Nanotube/Graphene Free-standing Electrodes for High Performance Lithium Batteries. *Adv. Funct. Mater.* **2013**, *23*, 1037−1045.
(18) Ge, X.; Liu, Y.; Goh, F. W.; Hor, T. S.; Zong, Y.; Xiao, P.; Zhang, Z.; Lim, S. H.; Li, B.; Wang, X.; Liu, Z. Dual-Phase Spinel $MnCo_2O_4$ and Spinel $MnCo_2O_4$/Nanocarbon Hybrids for Electrocatalytic Oxygen Reduction and Evolution. *ACS Appl. Mater. Interfaces* **2014**, *6*, 12684−12691.
(19) Park, J. B.; Lee, J.; Yoon, C. S.; Sun, Y. K. Ordered Mesoporous Carbon Electrodes for Li−O_2 Batteries. *ACS Appl. Mater. Interfaces* **2013**, *5*, 13426−13431.
(20) Tran, C.; Yang, X. Q.; Qu, D. Investigation of the Gas-Diffusion-Electrode Used as Lithium/Air Cathode in Non-Aqueous Electrolyte and the Importance of Carbon Material Porosity. *J. Power Sources* **2010**, *195*, 2057−2063.
(21) Lim, H. D.; Park, K. Y.; Song, H.; Jang, E. Y.; Gwon, H.; Kim, J.; Kim, Y. H.; Lima, M. D.; Ovalle Robles, R.; Lepro, X.; Baughman, R. H.; Kang, K. Enhanced Power and Rechargeability of a Li−O_2 Battery Based on a Hierarchical-Fibril CNT Electrode. *Adv. Mater.* **2013**, *25*, 1348−1352.
(22) Mitchell, R. R.; Gallant, B. M.; Thompson, C. V.; Shao-Horn, Y. All-Carbon-Nanofiber Electrodes for High-Energy Rechargeable Li−O_2 Batteries. *Energy Environ. Sci.* **2011**, *4*, 2952−2958.
(23) Thotiyl, M. M. O.; Freunberger, S. A.; Peng, Z.; Bruce, P. G. The Carbon Electrode in Nonaqueous Li−O_2 Cells. *J. Am. Chem. Soc.* **2013**, *135*, 494−500.
(24) McCloskey, B. D.; Speidel, A.; Scheffler, R.; Miller, D. C.; Viswanathan, V.; Hummelshøj, J. S.; Nørskov, J. K.; Luntz, A. C. Twin Problems of Interfacial Carbonate Formation in Nonaqueous Li−O_2 Batteries. *J. Phys. Chem. Lett.* **2012**, *3*, 997−1001.
(25) McCloskey, B. D.; Valery, A.; Luntz, A. C.; Gowda, S. R.; Wallraff, G. M.; Garcia, J. M.; Mori, T.; Krupp, L. E. Combining Accurate O_2 and Li_2O_2 Assays To Separate Discharge and Charge Stability Limitations in Nonaqueous Li−O_2 Batteries. *J. Phys. Chem. Lett.* **2013**, *4*, 2989−2993.
(26) Black, R.; Lee, J. H.; Adams, B.; Mims, C. A.; Nazar, L. F. The Role of Catalysts and Peroxide Oxidation in Lithium−Oxygen Batteries. *Angew. Chem., Int. Ed.* **2013**, *52*, 392−396.
(27) Itkis, D. M.; Semenenko, D. A.; Kataev, E. Y.; Belova, A. I.; Neudachina, V. S.; Sirotina, A. P.; Havecker, M.; Teschner, D.; Knop-Gericke, A.; Dudin, P.; Barinov, A.; Goodilin, E. A.; Shao-Horn, Y.; Yashina, L. V. Reactivity of Carbon in Lithium−Oxygen Battery Positive Electrodes. *Nano Lett.* **2013**, *13*, 4697−4701.
(28) Nakanishi, S.; Mizuno, F.; Abe, T.; Iba, H. Enhancing Effect of Carbon Surface in the Non-Aqueous Li−O_2 Battery Cathode. *Electrochemistry* **2012**, *80*, 783−786.
(29) Nakanishi, S.; Mizuno, F.; Nobuhara, K.; Abe, T.; Iba, H. Influence of the Carbon Surface on Cathode Deposits in Non-Aqueous Li−O_2 Batteries. *Carbon* **2012**, *50*, 4794−4803.
(30) Guo, X. X.; Zhao, N. The Role of Charge Reactions in Cyclability of Lithium−Oxygen Batteries. *Adv. Energy Mater.* **2013**, *3*, 1413−1416.
(31) Wang, H. Y.; Lu, T.; Meng, F. H.; Zhu, H. Q.; Liu, X. Y. Enhanced Osteoblast Responses to Poly Ether Ether Ketone Surface Modified by Water Plasma Immersion Ion Implantation. *Colloids Surf., B* **2014**, *117*, 89−97.
(32) Fan, W. G.; Cui, Z. H.; Guo, X. X. Tracking Formation and Decomposition of Abacus-Ball-Shaped Lithium Peroxides in Li−O_2 Cells. *J. Phys. Chem. C* **2013**, *117*, 2623−2627.
(33) Cui, Z. H.; Guo, X. X. Manganese Monoxide Nanoparticles Adhered to Mesoporous Nitrogen-Doped Carbons for Nonaqueous Lithium−Oxygen Batteries. *J. Power Sources* **2014**, *267*, 20−25.
(34) Bott, A. W. Practical Problems in Voltammetry 3: Reference Electrodes for Voltammetry. *Curr. Sep.* **1995**, *14*, 64−68.
(35) Dresselhaus, M. S.; Dresselhaus, G.; Jorio, A.; Filho, A. G. S.; Saito, R. Raman Spectroscopy on Isolated Single Wall Carbon Nanotubes. *Carbon* **2002**, *40*, 2043−2061.
(36) Singh, C.; Shaffer, M. S. P.; Windle, A. H. Production of Controlled Architectures of Aligned Carbon Nanotubes by an Injection Chemical Vapour Deposition Method. *Carbon* **2003**, *41*, 359−368.
(37) Trahan, M. J.; Mukerjee, S.; Plichta, E. J.; Hendrickson, M. A.; Abraham, K. M. Studies of Li−Air Cells Utilizing Dimethyl Sulfoxide-Based Electrolyte. *J. Electrochem. Soc.* **2012**, *160*, A259−A267.
(38) Chu, H. B.; Shen, Y. H.; Lin, L.; Qin, X. J.; Feng, G.; Lin, Z. Y.; Wang, J. Y.; Liu, H. C.; Li, Y. Ionic-Liquid-Assisted Preparation of Carbon Nanotube-Supported Uniform Noble Metal Nanoparticles and Their Enhanced Catalytic Performance. *Adv. Funct. Mater.* **2010**, *20*, 3747−3752.
(39) McCloskey, B. D.; Bethune, D. S.; Shelby, R. M.; Mori, T.; Scheffler, R.; Speidel, A.; Sherwood, M.; Luntz, A. C. Limitations in Rechargeability of Li−O_2 Batteries and Possible Origins. *J. Phys. Chem. Lett.* **2012**, *3*, 3043−3047.